Liquid phase epitaxial growth of InGaAs on InP using rare-earth-treated melts

Wei Gao[a] and Paul R. Berger[b]
Department of Electrical Engineering, University of Delaware, Newark, Delaware 19716

Matthew H. Ervin, Jagadeesh Pamulapati, Richard T. Lareau, and Stephen Schauer[c]
U.S. Army Research Laboratory, Physical Science Directorate, Fort Monmouth, NJ 07703-5601

(Received 3 July 1996; accepted for publication 10 September 1996)

High-quality $In_{0.53}Ga_{0.47}As$ epilayers have been grown on semi-insulating (100) Fe-doped InP substrates. The growths were performed by liquid phase epitaxy (LPE) using rare-earth-doped melts in a graphite boat. The rare-earth elements studied were Yb, Gd and Er which act as gettering agents of impurities. Hall measurements show an elevated electron mobility for rare-earth-treated samples over undoped samples, $\mu_e = 11\,470$ cm^2/V s at 300 K and reduced carrier concentration (n-type), 9.33×10^{13} cm^{-3}. The Hall results indicate an improvement in layer quality, but suggests that the treated layers are compensated. Photoluminescence (PL) studies show that the layers grown from rare-earth-doped melts have higher integrated PL efficiency with narrower PL linewidths than the undoped melt growths. The grown materials were fully characterized by Fourier transform infrared spectroscopy, double-crystal x-ray diffraction, energy dispersive spectroscopy, secondary-ion-mass spectroscopy, and deep level transient spectroscopy (DLTS). Compositional measurements reveal no measurable incorporation of rare-earth elements into the grown epilayers. DLTS measurements indicate the creation of two deep levels with rare-earth treatment, which is attributed to either the rare earth elements or impurities from within the rare-earth elements. Subsequent glow discharge mass spectrometry measurements reveal many impurities within the rare-earth elements which preferentially might lead to p-type doping centers and/or deep levels. Thus, rare-earth doping of LPE melts clearly improves epitaxial layer quality, however, the purity of commercially available rare-earth elements hinders optimal results. [S0021-8979(96)00224-1]

I. INTRODUCTION

The $In_{0.53}Ga_{0.47}As$ material system is very important for modulation-doped field-effect transistors (MODFET) used in monolithic microwave integrated circuits (MMIC) and avalanche photodiodes (APD), *p-i-n* photodiodes and metal–semiconductor–metal (MSM) photodiodes used in long wavelength ($1.3\ \mu m \leqslant \lambda \leqslant 1.55\ \mu m$) lightwave communications. For these applications, the $In_{0.53}Ga_{0.47}As$ material needs to be of high quality and low carrier concentration. Liquid phase epitaxy (LPE) is a well developed and proven technique to grow compound semiconductor materials. High quality layers are possible with LPE with a minimum of capital investment when compared to alternative techniques such as molecular-beam epitaxy (MBE) and metal-organic chemical vapor deposition (MOCVD). LPE inherently provides high-quality material since growth is at reduced temperatures and closer to thermodynamic equilibrium, thus achieving near perfect crystallinity and purity. LPE remains a viable option for the production of optoelectronic materials and devices.[1,2]

However, one problem with LPE growth is the unavoidable impurities which arise from the melt and growth ambient. It has now been recognized that Si and S are the two major background donor impurity species present in the In and InP, and that C is the principal acceptor, originating from the graphite boat.[3] Various methods have been used to reduce the concentration of the residual impurities. Extended hydrogen baking of the In melt and the source solution (formed by adding InAs and GaAs) is widely known to lower the levels of both donor (Si and S)[4] and acceptor (Al, Mg, Zn)[5] impurities in the grown epitaxial layer. Bhattacharya *et al.*[6] showed electron mobilities significantly improved upon hydrogen baking the entire melt after the In slug was individually prebaked with hydrogen. Also, Bagraev *et al.*[7] used a sapphire boat to reduce the background doping and further enhance the electron mobility, but, Bagraev *et al.*[7] also discovered that the addition of trace amounts of rare-earth elements to LPE growth melts could significantly reduce the background doping level and increase the electron mobility.

Recent studies have shown that impurities (for example, S, Se, Si, C, Te, O, etc.) in III–V semiconductors form stable compounds with rare earth elements and that these rare-earth compounds are insoluble in indium (In), the common solvent used in LPE growth of InGaAs. Thus, rare-earth elements can be used to remove these impurities from the InGaAs LPE growth melts and reduce the background doping of grown epilayers. Also, it was found that the rare-earth elements do not incorporate into the epitaxial layer at reduced growth temperatures, similar to those used in this study. Thus, the reader is cautioned that the LPE melt is doped with

[a]Present address: Laserton, 11 Oak Park, Bedford, MA 01730.
[a]Electronic mail: pberger@ee.udel.edu
[c]Present address: Motorola, 1300 North Alma School Road, Chandler, AZ 85224.

 0021-8979/96/80(12)/7094/10/$10.00

rare-earth elements, but the epitaxial layer is not. The epitaxial layer will henceforth be referred to as undergoing a rare-earth treatment. One dilemma of this study is the limited purity of commercially available rare-earth elements (see Table IV). This leads to new impurities being introduced into the grown layers. The first rare-earth elements studied were La and Ba by Haigh,[8] and examples of more recent investigations of rare-earth-doped semiconductors concerning defects, doping, growth, theory, and optoelectronics can be found in the Materials Research Society Proceedings.[9]

II. EXPERIMENTAL PROCEDURES

We have grown $In_{0.53}Ga_{0.47}As$ on semi-insulating (100) InP:Fe substrates by LPE in a palladium diffused hydrogen ambient using a horizontal graphite sliding boat. A very low concentration of rare-earth element (Yb, Gd, and Er) was introduced into the In growth melts (about 10^{-4} mole fraction) to remove residual impurities from the melts.

Prior to this series of growth runs, the LPE quartz tube was etched in buffered hydrofluoric acid and thoroughly rinsed to remove surface contamination. Then, the quartz tube was outgassed at 1000 °C under a H_2 ambient. The graphite boat was soaked in aqua regia, $HCl:HNO_3$ (3:1), for 100 h followed by a hot de-ionized (DI) water rinse until the waste water reached a pH of 7. The graphite boat was then baked at 900 °C under vacuum or H_2 for 50 h to remove residual impurities.

After cleaning the LPE system, pure indium (99.9999%) was loaded into the graphite sliding boat, and then various In melt, and later growth melt, bakeout schemes were used to obtain high-quality crystals. The In melts were baked out at 710 °C ranging from 6 to 115 h in an ultrapure H_2 ambient. The system was then cooled down to room temperature and appropriate amounts of polycrystalline GaAs and InAs were added to the growth melt to form the growth solution. The liquid solution compositions, $X^l_{Ga}=2.52\times10^{-2}$ atomic fraction and $X^l_{As}=5.66\times10^{-2}$ atomic fraction, were used to grow lattice-matched $In_{0.53}Ga_{0.47}As$ on semi-insulating (100) InP:Fe substrates. The growth solution was baked out at 680 °C in an ultrapure H_2 ambient for 1.5–20 h. The system was cooled to room temperature and a polished and cleaned (100) InP:Fe substrate was loaded into the boat. A proximity cap InP wafer was used to prevent phosphorus evaporation from the substrate prior to epitaxy. The system was heated up to 650 °C for 30 min and then lowered to the growth temperature of 630 °C where supercooled growth was initiated. Supercooled LPE growth is a hybrid LPE growth technique which initially uses a step-cooled temperature step to enhance nucleation on the substrate, but then growth becomes ramp cooled in the later stages for thicker layers. An initial supersaturation of 8 °C was used followed by a constant cooling rate of 0.5 °C/min. Figure 1 depicts schematically the growth process used. The same LPE growth melt was used for three or more consecutive runs. The thickness of the epitaxial layers ranged from 1 to 12 μm depending on the growth time employed.

A total of 64 LPE growth runs for $In_{0.53}Ga_{0.47}As$ on InP were performed. The grown epitaxial layers were characterized by various measurements. Optical microscopy and in some cases scanning electron microscopy (SEM) was used to perform a visual inspection of the surface morphology. Fourier transform infrared spectroscopy (FTIR) was used to measure the room temperature band gap. Lattice-mismatch, $\Delta a/a$, was measured by double-crystal x-ray diffraction. Low temperature photoluminescence (PL) measurements were performed to analyze the optical quality of the $In_{0.53}Ga_{0.47}As$ layers. Hall measurements were used to measure the background carrier concentration and electron mobility of the $In_{0.53}Ga_{0.47}As$ layers. Energy dispersive spectroscopy (EDS) was used to measure composition and the incorporation of rare-earth elements into the epilayers. Secondary-ion-mass spectroscopy (SIMS) measurements were used to measure the incorporation of rare-earth elements and the level of residual impurities in the undoped and rare-earth-treated layers. Temperature-dependent capacitance–voltage (C–V) profiling and deep level transient spectroscopy (DLTS) measurements were used to measure the creation of deep levels by the rare-earth species or associated impurities. Lastly, glow discharge mass spectrometry (GDMS) was used to analyze the impurity levels in the rare-earth foils used as dopants to the LPE melts.

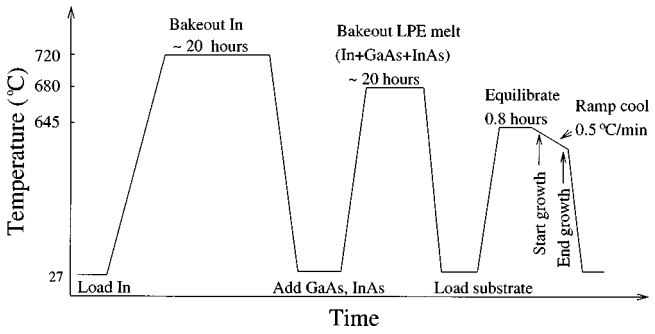

FIG. 1. LPE growth temperature cycles and process.

III. RESULTS AND DISCUSSION

A. Surface microscopy

A Leica (Leitz Ergolux AMC) optical microscope with Nomarski interference contrast was used to examine the postgrowth surface morphology. Nomarski microscopy utilizes the interference of polarized light to enhance the surface contrast without detectable loss of resolution. A slight change in optical path difference results in a noticeable color change, hence an interference contrast results.

For direct comparison to earlier growths, the rare-earth elements were only added to the LPE melt on the third growth run after generating a couple of undoped control samples. In this way, slight variances from one LPE melt to the next will not be reflected in direct comparisons of undoped and rare-earth-treated layers. Ytterbium (Yb), gadolinium (Gd), and erbium (Er) were used interchangeably as the rare-earth elements. Overall trends using any one of the rare-earth species were quite similar, so the data presented here is a mixture from among the 64 generated samples using Yb, Gd, and Er elements. A relatively high rare earth

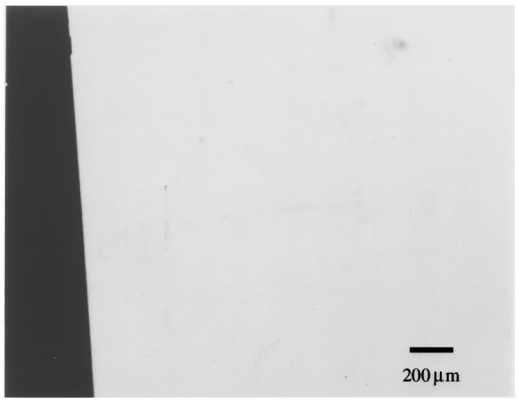

(a)

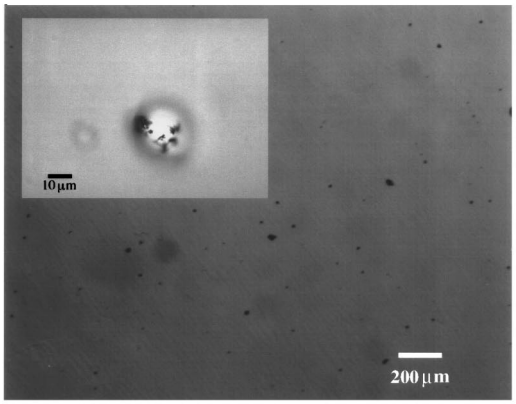

(b)

FIG. 2. Nomarski optical photomicrographs showing the surface morphology of (a) an undoped $In_{0.53}Ga_{0.47}As$ epitaxial layer (P24-1) grown on InP and (b) an $In_{0.53}Ga_{0.47}As$ layer (P18-3) grown from an Er-doped LPE melt. A SEM photomicrograph [inset of (b)] shows a magnified view of a particulate on the surface morphology of the $In_{0.53}Ga_{0.47}As$ layer (P18-3) grown with Er-doped LPE melt.

concentration of 4.6×10^{-4} atomic fraction resulted in a poor surface morphology with many defect sites. When the rare-earth concentration was reduced to 1×10^{-4} atomic fraction or below, the surface morphology was greatly improved. However, morphologically there still exist more defect sites with rare-earth treatment than earlier undoped growths from the same melt. It is believed that due to the high reactivity of the rare-earth elements, they react with impurities within the LPE melt and precipitate out as a slag atop the LPE melt. It is believed that sometimes nodules of these precipitates incorporate into the epitaxial layer creating the observed morphological defects. EDS analysis of these defects indicates that these nodules are high concentrations of impurity species as well as the constituent rare-earth species.

Figures 2(a) and 2(b) are Nomarski photomicrographs of $In_{0.53}Ga_{0.47}As$ layers grown without and with rare-earth treatment, respectively. An examination of an undoped $In_{0.53}Ga_{0.47}As$ sample (P24-1) in Fig. 2(a) reveals one of the better grown crystals. The entire surface is virtually mirror smooth and free of blemishes. Figure 2(b) is another Nomarski photomicrograph of an $In_{0.53}Ga_{0.47}As$ layer (P18-3) grown after Er treatment. Note the appearance of specks or blemishes on the surface. Figure 2(b) inset shows a SEM photomicrograph of the same layer (P18-3) focusing in upon one of these particulate centers. The defect site appears to lie mostly on top of the wafer and be only slightly submerged into the epitaxial layer.

TABLE I. Bandgap and composition of undoped and Yb-treated $In_xGa_{1-x}As$ measured by FTIR.

Epitaxial layer	Sample number	Rare-earth concentration	E_g (eV)	x	$\Delta a/a$ (%)
$In_xGa_{1-x}As$	P9-1	0	0.7302	0.520	−0.0832
$In_xGa_{1-x}As$	P9-2	0	0.7166	0.533	+0.0066
$In_xGa_{1-x}As$	P9-3	Yb:2.3×10^{-4}	0.7073	0.542	+0.0687
$In_xGa_{1-x}As$	P24-1	0	0.72808	0.522	−0.0693
$In_xGa_{1-x}As$	P24-4	Yb:5.7×10^{-5}	0.7298	0.521	−0.0798

B. Fourier transform infrared spectroscopy

The room-temperature absorption of the grown samples was measured by Fourier transform infrared spectroscopy (FTIR) (Nicolet 740 FTIR spectrometer) using a quartz beam splitter and a PbSe detector. FTIR is a simple and direct method to measure the room-temperature bandgap which is determined from the absorption edge. The transmission through the thin epilayer and the substrate was measured. Substrate absorption was removed by ratioing the data to a bare InP substrate. Absorption curves were extrapolated, and the band gap of the material estimated. The Ga and In compositions can then be computed following the empirical formula below which relates $In_xGa_{1-x}As$ composition to the lowest direct energy gap E_g at room temperature,[10]

$$E_g^{300\ \mathrm{K}}(\mathrm{In}_x\mathrm{Ga}_{1-x}\mathrm{As}) = 1.42 - 1.615x + 0.555x^2. \quad (1)$$

The effects of lattice-mismatch strain energy on the band gap in Eq. (1), as noted by Kuo *et al.*[11] and Bassignana *et al.*,[12] were not taken into account, but are a best fit curve to published data. Table I lists the measured bandgap, x value, and lattice mismatch of $In_{0.53}Ga_{0.47}As$ samples P9-1, P9-2, P9-3, P24-1, and P24-4. The P9 series and P24 series were each grown consecutively using the same melts (In+GaAs+InAs) with the exception that Yb was added to the melt prior to the growth of samples P9-3 and P24-4. It was found that, at the low Yb doping levels employed in this study, that the rare-earth element did not distort the crystal lattice measurably and therefore did not affect the host crystal structure or bandgap energy.

C. Double-crystal x-ray diffraction

Double-crystal x-ray diffraction was used for the extraction of the lattice mismatch. Double-crystal x-ray diffraction utilizes two successive Bragg reflections off two independent crystal lattices. The Philips XRG 3100 x-ray generator and APD 3520 x-ray-diffraction control system were used for this analysis. The condition for constructive interference is given by Bragg's law,

$$2d \sin \theta_B = n\lambda, \quad (2)$$

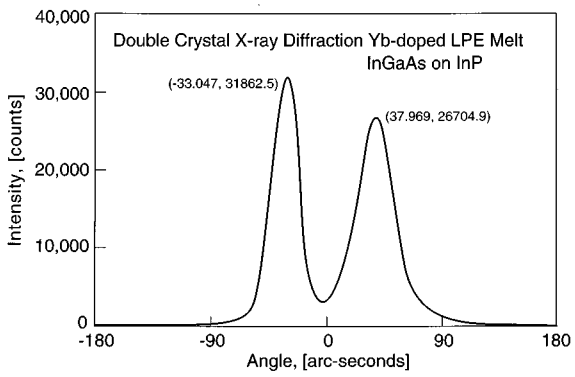

FIG. 3. Double-crystal x-ray diffraction of $In_{0.53}Ga_{0.47}As$ on InP (P11-3) grown by LPE using an Yb-doped LPE melt.

where d is the lattice constant, θ_B is the incident angle, and n is an integer representing the diffraction order.

Double-crystal x-ray diffraction can measure a very small lattice mismatch, which is a very important factor for compound semiconductor growth. A high-quality crystal is expected for a lattice mismatch below 0.3 %. The x-ray sources used were generated from a Cu target, which has the following characteristic wavelengths $K\alpha_1$, 1.5443 Å and $K\alpha_2$, 1.5405 Å. Typical diffraction spectra from single semiconductor layer structures exhibit a rocking curve consisting of two principal peaks. One principal peak is from the epitaxial layer and the other is from the substrate. Figure 3 shows the double-crystal x-ray diffraction spectrum for one of the more mismatched layers, and therefore shows the epilayer and substrate peaks clearly resolved. By solving Eq. (2), the lattice constant can be found. To do so, insert $n = 4$, for the (400) reflection order, d as the lattice constant (a_{epi}), θ_B as 31.668 59°, the reference Bragg angle of the InP substrate, and λ as 1.5405 Å, the x-ray wavelength of the Cu source. Then, the lattice constant and, therefore, mismatch, can be calculated from the following equation:

$$a_{\text{epi}}(\text{on InP}) = \frac{4 \times 1.5405}{2 \sin\left[\frac{1}{2}\left(2 \times 31.668\ 59 \pm \frac{\Delta\omega}{3600}\right)\right]}\text{Å}, \qquad (3)$$

where $\Delta\omega$ is the separation angle of the two peaks measured in arcsec. Consequently, from a simple linear interpolation between the binary alloys of InAs and GaAs, the lattice constant of $In_xGa_{1-x}As$ versus the atomic fraction x obeys the following relation,

$$a_{\text{epi}}(\text{on InP}) = a_{In_xGa_{1-x}As} = 0.4051x + 5.6533\ \text{Å}. \qquad (4)$$

Thus, the stoichiometry of the epilayers can be deduced. The results of double-crystal x-ray-diffraction measurements of several layers are listed in Table II. The data show excellent lattice matching which was routinely achieved over the 64 growth runs. From Table II, again there is no evidence indicating the rare earth element is distorting the overall $In_{0.53}Ga_{0.47}As$ crystal structure which suggests the rare-earth element does not incorporate into the $In_{0.53}Ga_{0.47}As$ epilayer.

TABLE II. Lattice parameter and composition of undoped and Yb-treated $In_xGa_{1-x}As$ measured by double-crystal x-ray diffraction. T_1 is In bakeout time (h); T_2 is the solution (In + InAs + GaAs) bakeout time (h).

Epilayer	Sample	Dopant	T_1/T_2	$\Delta a/a$ (%)	x
$In_xGa_{1-x}As$	P9-1	none	84/ 8	−0.0155	0.5294
$In_xGa_{1-x}As$	P10-1	none	13/ 2	−0.0210	0.5289
$In_xGa_{1-x}As$	P10-3	Yb	13/ 2	−0.0141	0.5297
$In_xGa_{1-x}As$	P11-1	none	13/11	+0.0066	0.5335
$In_xGa_{1-x}As$	P11-3	Yb	13/11	−0.0348	0.5273

D. Photoluminescence

Low-temperature photoluminescence (PL) spectra were recorded using a dispersive 1 m high-resolution Jarell–Ash (Czerny–Turner) monochrometer and detected by a liquid-nitrogen-cooled Ge *p-i-n* photodetector (North Coast EO-817L). The samples were mounted on a cold finger in a temperature variable helium-flow cryostat. Excitation was provided by a multiline cw argon laser (488–514 nm). Data collection and lock-in amplification were controlled by a desk-top computer.

Figure 4 is the photoluminescence spectra of P11-1 and P11-3 samples at 5.5 K. P11-1 is undoped $In_{0.53}Ga_{0.47}As$, while P11-3 is grown from a Yb-doped LPE melt. The two characteristic PL peaks are at 1.531 μm (0.810 eV) and 1.564 μm (0.793 eV), respectively. The main peak at 0.810 eV is attributed to a bound exciton to donor transition and the 0.793 eV peak is assigned as a conduction-band to acceptor impurity level transition, probably a carbon-related defect. In general, luminescent efficiency and, therefore, intensity, increases with increasing purity of the crystal. The intensity of the 0.81 eV peak for the Yb-treated $In_{0.53}Ga_{0.47}As$ (P11-3) is 2.1 times higher than the intensity of the same peak for the undoped $In_{0.53}Ga_{0.47}As$ (P11-1). The full width at half-maximum (FWHM), which indicates the amount of broadening mechanisms present, were 4.5 and 6 meV for P11-3 and P11-1, respectively. These results clearly indicate that $In_{0.53}Ga_{0.47}As$ grown from rare-earth-doped LPE melts is of higher purity than undoped $In_{0.53}Ga_{0.47}As$.

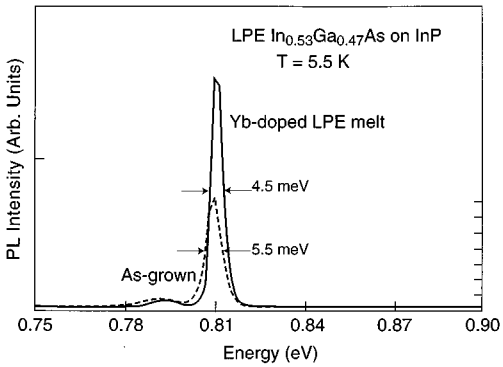

FIG. 4. Low-temperature photoluminescence spectra of $In_{0.53}Ga_{0.47}As$ on InP grown from an undoped $In_{0.53}Ga_{0.47}As$ (P11-1) and Yb-treated $In_{0.53}Ga_{0.47}As$ (P11-3). The addition of Yb doping to the LPE melt clearly increases PL intensity and narrows the linewidth. No Yb PL signal was observed, indicating very little incorporation of Yb to the epitaxial film.

TABLE III. Hall measurements of undoped and Gd-treated $In_{0.53}Ga_{0.47}As$ showing dramatic improvement in mobility and carrier concentration after addition of the rare-earth element to the LPE melt. μ is the mobility (cm^2/V s), T_1 is the indium bake time (h), T_2 is the melt solution (InAs + GaAs + In) bake time (h), and n is the carrier concentration (cm^{-3}).

Epitaxial layer	Melt dopant	T_1 / T_2	n (300 K)	μ (300 K)	n (77 K)	μ (77 K)
$In_{0.53}Ga_{0.47}As$	none	62/13	4.48×10^{15}	9942	3.71×10^{15}	21 233
$In_{0.53}Ga_{0.47}As$	Gd	115 /18	9.33×10^{13}	11 470	4.65×10^{13}	37 823

It should also be noted that the luminescence peak from Yb near the wavelength of 1.0 μm (1.24 eV)[13] due to the 4f–4f shell transition was not observed. This suggests that no appreciable amount of rare-earth element was incorporated into the epitaxial layer. This is expected at the low growth temperatures and low LPE melt rare earth concentration levels employed for this series of experiments. However, due to the band gap of $In_{0.53}Ga_{0.47}As$ ($E_g \sim 0.8$ eV), there may be significant self-absorption of the 1.24 eV photons emitted from the Yb centers. Further clarification on the incorporation of rare-earth elements is presented below using EDS and SIMS measurements.

E. Hall measurements

The free carrier concentrations and Hall electron mobilities in the epitaxial layers were measured at room and liquid nitrogen (77 K) temperatures using the van der Pauw technique. Cloverleaf structures were defined photolithographically on the InGaAs samples. Mesa isolation was achieved by using a phosphoric acid etchant. The samples were etched in H_3PO_4:H_2O_2:H_2O (1:1:8) for several minutes with an etching rate of 0.6 μm/min. The InP substrate acts as a stop-etch layer for this etchant, therefore, controlled etching is possible. Since the InP substrates employed in this study were all of the semi-insulating type, parallel conduction through the InP substrate is not expected to skew the measured data. The $In_{0.53}Ga_{0.47}As$ samples were generally several microns thick, thus avoiding surface depletion effects for low-doped layers. Measurements were performed with a current of 50 μA, magnetic field of 3000 G, and the Hall factors were calculated individually.

Table III lists the Hall measurement results for two grown samples. It was found that both the carrier concentration (n type) and mobility were considerably improved after Gd treatment of the LPE melt. The room-temperature carrier concentration dropped from 4.48×10^{15} to 9.33×10^{13} cm^{-3} and room-temperature electron mobility increased from 9940 to 11 470 cm^{-2} V^{-1} s^{-1}. This is a significant improvement and strongly suggests that Gd played an important role in the improvement. Gd is a very reactive element. Gd interacts strongly with S, Si, C, and O impurities in the melt. As is discussed below, SIMS results show that Si, S, and C levels were reduced after the rare-earth treatment.

Gorelenok *et al.*[14] performed Hall measurements on LPE-grown wafers using rare-earth element doped LPE melts in the temperature range 77–300 K. They found no temperature dependence of the electron concentration, indicating little compensation. Analysis of our samples reveals a slight variation in carrier concentration with change in temperature for the undoped $In_{0.53}Ga_{0.47}As$, but a much larger shift for the Gd-treated $In_{0.53}Ga_{0.47}As$ sample. This is suggestive that the Gd-treated sample is compensated.

The rare-earth elements in the LPE melt interact strongly with carbon and oxygen forming electrically inactive centers consisting of oxides and carbides.[7] Thus, the rare-earth species reduce the shallow donors created from Si_xC_y, Si_xO_y, and C_xO_y making the epitaxial layer lower in carrier concentration. For this reason, it is expected that the mobility would be elevated due to reduced ionized impurity scattering and the carrier concentration would be reduced.

It should be mentioned that the low-temperature mobility is less than optimum, and the carrier concentration for the Gd-treated sample is almost too low to be credible for this low-band-gap material. Since Hall measurements only probe the difference N_D-N_A, the net carrier concentration, it is expected that the rare-earth-treated samples have a high degree of compensation. The overall mobility trend, however, testifies to the reduction in n-type doping upon use of rare earth species, but suggests a possible enhancement in p-type doping centers leading to a low N_D-N_A. Furthermore, since the low field mobility is enhanced upon rare-earth treatment, the overall impurity sites, N_D+N_A, must be reduced upon rare-earth treatment because less impurity scattering is taking place.

F. Energy dispersive x-ray spectroscopy and secondary ion mass spectroscopy

Energy dispersive x-ray spectroscopy (EDS) analysis was performed on some of the samples, and within the limited detection range of EDS no rare element was detected for the rare-earth-treated layers in the bulk epitaxial layer. Further compositional analysis using the more sensitive secondary ion mass spectroscopy (SIMS) analysis (detailed below) was also performed which supports this supposition. This indicates the low solubility of rare-earth elements in the indium melt at the low growth temperatures employed for this study (i.e., 630 °C). For instance, Körber *et al.*[15] needed 800 °C to incorporate Yb into an InP epitaxial layer. High concentrations of rare-earth elements were, however, detected within small defect sites on the grown surface. These defects are, as mentioned earlier, thought to be due to rare-earth compound precipitations during the growth process.

SIMS analysis was also performed on a series of $In_{0.53}Ga_{0.47}As$ layers grown from undoped and rare-earth-doped LPE melts. SIMS analysis also did not detect any rare-earth elements incorporated in the epilayers. SIMS characterization searched for elemental rare-earth species, and revealed no signal above the noise or among the interferences for all epilayers scanned. In addition, SIMS analysis also performed a thorough examination of the impurity levels of a number of electrically active species. Figures 5(a) and 5(b) show SIMS depth profiling data for an undoped and Yb-treated $In_{0.53}Ga_{0.47}As$ layer, respectively, and Figs. 6(a) and 6(b) also show SIMS depth profiling data for an undoped and Gd-treated $In_{0.53}Ga_{0.47}As$ layer, respectively. In all of these scans, the species In, O, C, S, Cu, Fe, and Si were

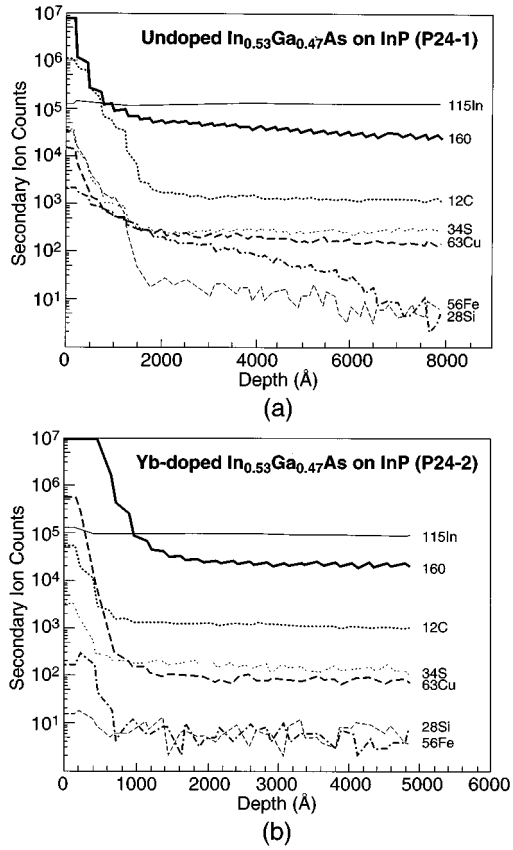

FIG. 5. Secondary-ion-mass spectra as a function of depth for (a) an undoped $In_{0.53}Ga_{0.47}As$ epilayer on InP and (b) an $In_{0.53}Ga_{0.47}As$ epilayer grown from the same LPE melt after the LPE melt was doped with Yb.

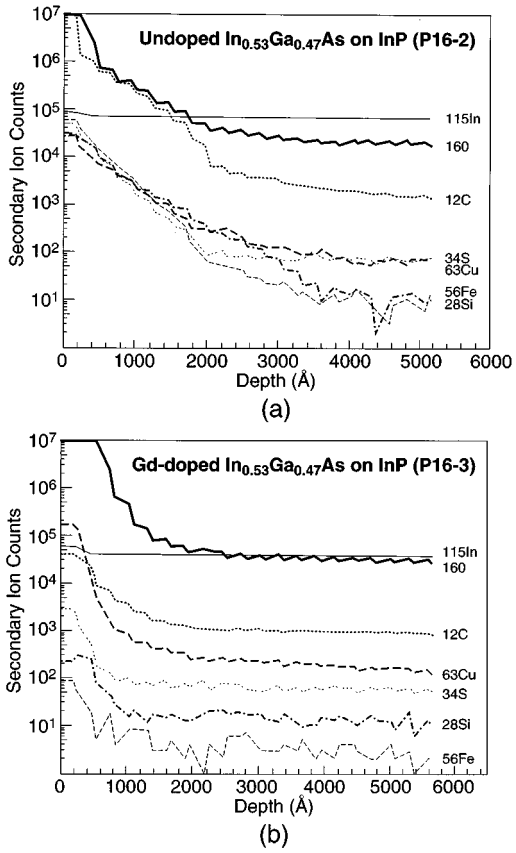

FIG. 6. Secondary-ion-mass spectra as a function of depth for (a) an undoped $In_{0.53}Ga_{0.47}As$ epilayer on InP and (b) an $In_{0.53}Ga_{0.47}As$ epilayer grown from the same LPE melt after the LPE melt was doped with Gd.

tracked as a function of depth to about 5000–8000 Å below the surface. Both data sets reveal similar signatures of impurities. There is a noticeable segregation of impurities to the surface of all the epilayers.

Since the LPE growth process used in this study is the supercooled method, the growth rate is expected to be initially rapid and then exponentially decay to a steady-state rate. For most of the growth runs, the growth process is typically terminated before a steady-state value can be reached. This nonlinear growth rate could cause segregation of impurities to the surface during the slower growth rate. Or, this accumulation at the surface may be attributed to the final growth sequence when the melt is being pulled away from the substrate to terminate growth. Generally, impurities which have low solubilities within the In-based LPE melt will accumulate at the LPE melt surface as slaglike solid matter. Perhaps the pulling action of removing the melt from the wafer disturbs this separation and causes a cascade of impurity particulates to mix with the LPE melt and incorporate into the final surface of the LPE epilayer. This impurity accumulation is confined to the upper 1000–2000 Å of the epilayer. As can be seen below in image plots, much of the impurity incorporation is not evenly distributed as would be the case if the impurity species were soluble in the In melt and evenly mixed throughout.

After the SIMS analysis probes past the uppermost 3000 Å of the epilayer, a steady-state impurity level is reached. From inspection of the overall signatures of the impurity species scanned, shown in Figs. 5 and 6, it is clear that regardless of rare-earth dopant species used, there is an overall reduction of impurity levels. The only exception is the O peak. There seem to be significantly higher levels of O at the surface of the rare-earth-treated samples. This is perhaps to be expected, since the rare-earth species readily oxidize upon opening the vendor's package. Rare-earth elements are difficult to clean prior to introduction into the LPE melt other than a simple degreasing procedure. Some rare-earth elements can even spontaneously combust. Therefore, no effort was made to remove the surface oxide from the rare-earth elements before adding to the LPE melts.

SIMS depth profiling shows some noticeable reduction in impurities such as C, S, and Cu, but an almost complete elimination, to the detection limit, for species such as Si and Fe in rare-earth treated samples. In addition, the high concentrations of impurities observed to accumulate in $\sim$ 2000 Å deep from the surface for the undoped samples is reduced in depth. A surface accumulation layer is still present for the rare-earth-treated samples, but it is confined to a shallower region ($\leqslant$ 1000 Å) and does not rise to impurity levels as high as seen at the surface of the undoped InGaAs samples.

Lastly, Figs. 7(a) and 7(b) represent spatial image plots of SIMS scans for carbon species of the same $In_{0.53}Ga_{0.47}As$ samples and data runs shown previously in Fig. 6. The images shown were taken from an approximate

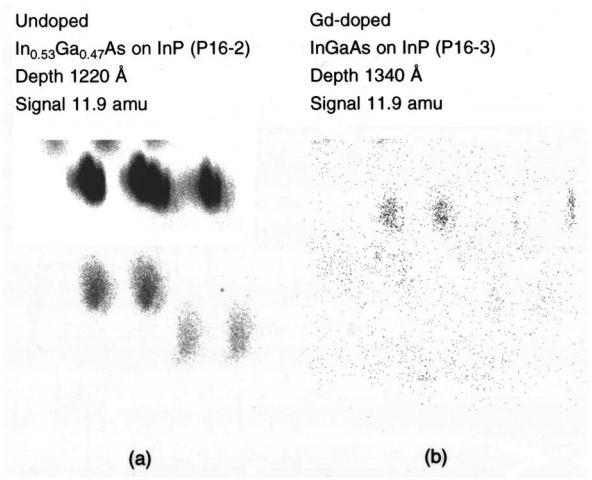

FIG. 7. Image data from secondary-ion-mass spectra for (a) an undoped and (b) Gd treated $In_{0.53}Ga_{0.47}As$ samples shown in Fig. 6 for carbon species at a depth of about 1000 Å. The images display the square of the measured particle counts as greyscale information. Note that the two images have been electronically altered for the reader to avoid a blank image appearing in (b). The actual disparity between the raw data for both images is more pronounced.

depth of 1300 Å to avoid surface contamination effects. Represented in Fig. 7 is the spatial image data for carbon (12 u) when the beam is rastered across the etched crater. The images displayed are 190×190 μm^2. Note, that the images displayed in Figs. 7(a) and 7(b) have been electronically altered. The grey scale represented is related to the square of the measured particle count. The image in Fig. 7(b) was actually much weaker in intensity than Fig. 7(a), and therefore was enhanced to avoid depicting a blank image. Therefore, the disparity between the particle counts in Fig. 7(a) and Fig. 7(b) is actually much more dramatic when viewing the raw data. Again, it is clear that there is a reduction in the impurity species, in this case carbon, from the undoped $In_{0.53}Ga_{0.47}As$ shown in Fig. 7(a) to the Gd-treated $In_{0.53}Ga_{0.47}As$ shown in Fig. 7(b). Most significant, however, is the uneven distribution of impurities throughout the epilayers. Noticeable clumping of the impurity species is observed. Other image scans, not shown, for other detected impurities at other mass numbers show similar clustering in the same regions as these carbon clusters. The carbon image scans shown were chosen because they register the largest concentration variation that could be readily observed. It should be mentioned that the graphite LPE boat is a probable source of carbon contamination outside those intrinsic to the LPE melt ingredients. That is perhaps why the carbon SIMS images show a dramatic variation.

These clumps of impurities observed by SIMS are not in any way associated with the particulate defects previously focused upon in Fig. 2(b) inset when inspecting the surface morphology. There are three reasons to draw this conclusion. First, the undoped sample has a large density of clumps which are greatly reduced if not virtually eliminated after rare-earth treatment, whereas the surface particulate defects appeared only after rare-earth treatment. Second, SIMS was not able to detect any rare-earth elements residing inside these impurity clumps within the detection limit. Third, the density of clusters detected by SIMS is at a higher density than those particulates found under the microscope, although their overall diameters are comparable to the particulate shown in Fig. 2(b) inset. Thus, the impurities which incorporate into the epitaxial layer do so almost as a cluster of particulate matter, but, what is most significant is the dramatic drop in impurity species after rare-earth treatment of the LPE melt. Clearly, the rare-earth elements are gettering impurities and removing them from the epitaxial layer via insolubility in the LPE melt.

G. Deep level transient spectroscopy

To perform capacitance–voltage (C–V) and deep level transient spectroscopy (DLTS) measurement, a p^+–n^- junction structure was made on the unintentionally doped n^--$In_{0.53}Ga_{0.47}As$ layers grown on semi-insulating (SI) InP:Fe substrates. A p^+ layer was formed postgrowth by an Emulsitone spin-on-glass dopant (Zn). The SiO_x:Zn layer was first spun on the InGaAs layer, followed by a low-temperature curing process and a high-temperature rapid thermal annealing (RTA) diffusion. As the Zn diffused into the n^--$In_{0.53}Ga_{0.47}As$ layer, a p^+–n^- diode was formed. Following the diffusion, the SiO_x layer was removed by buffered hydrofluoric acid. The thickness of the p^+ layer is very sensitive to the diffusion time and temperature. A series of diffusions was performed for this study by varying both temperature and time to control the diffusion depth. These samples were examined by SIMS and the results are presented elsewhere.[16] Diffusion at 750 °C for 40 s was found to be an optimal recipe for forming a shallow p^+–n^- junction without diffusing through most of the epilayer. Diodes were defined photolithographically and mesa isolation achieved by using the same etchant described in Sec. III E.

Both ohmic contacts were made by lift-off photolithography. The n-type ohmic contact was formed on the unintentially doped n^--$In_{0.53}Ga_{0.47}As$ layer with thermal evaporation of 800 Å Au–Ge (12% Ge), 200 Å Ni, 200 Å Ti, and 2000 Å Au, respectively, which were annealed in a RTA at 425 °C for 30 s in a forming gas ambient (15% H_2/85% N_2). The p-type ohmic contact was formed on the top p^+-$In_{0.53}Ga_{0.47}As$ layer with 500 Å Zn capped with 2000 Å Au using an electron-beam evaporation under high vacuum. The p-type contacts were nonalloyed. The junction areas are circular with 1 or 0.5 mm diameters defined by contact photolithography. The epitaxial $In_{0.53}Ga_{0.47}As$ layer thicknesses are 2 and 19 μm for P11-3 and P9-2, respectively. P9-2 is the undoped sample grown by LPE, and P11-3 was grown with an Yb-doped LPE melt with Yb concentration about 0.007%.

C–V measurements were performed prior to the DLTS measurements. Figures 8(a) and 8(b) show the carrier concentration versus voltage at various temperatures. Figure 8(a) shows little temperature dependence of the electron density in sample P9-2, which indicates an absence of deep levels. Figure 8(b) shows the C–V measurement results from sample P11-3. It clearly shows a temperature dependence of carrier concentration, which suggests the existence of deep levels. This was confirmed by subsequent DLTS results.

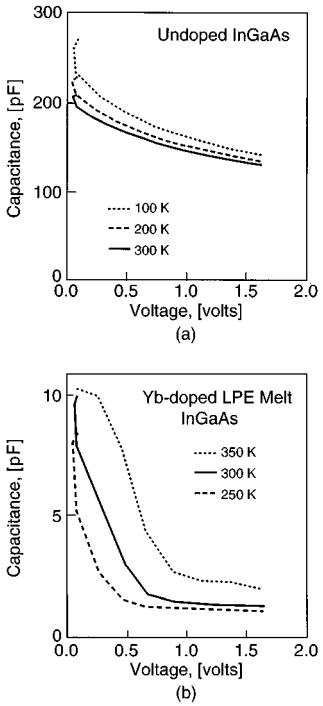

FIG. 8. Temperature dependent C–V measurements of $In_{0.53}Ga_{0.47}As$ grown from (a) undoped (P9-2) and (b) Yb-treated LPE melt (P11-3) on InP.

A BIO-RAD DL4600 DLTS system was used for the DLTS measurements. Figure 9 shows the DLTS signal observed in an undoped $In_{0.53}Ga_{0.47}As$ epitaxial layer (P11-1) and Yb-treated $In_{0.53}Ga_{0.47}As$ layer (P11-3) in the temperature range from 100 to 325 K. There were no deep levels observed in the undoped layer within the detection limit ($\Delta C/C \sim 10^{-4}$). Although electron traps have been observed for InGaAs layers grown by MBE[17,18] and at the heterointerfaces of InGaAs/InP grown by LPE[19,20] and MBE,[18] no deep levels have been documented in high-quality LPE-grown $In_{0.53}Ga_{0.47}As$ layer, as reported by Ogura *et al.*[20] and

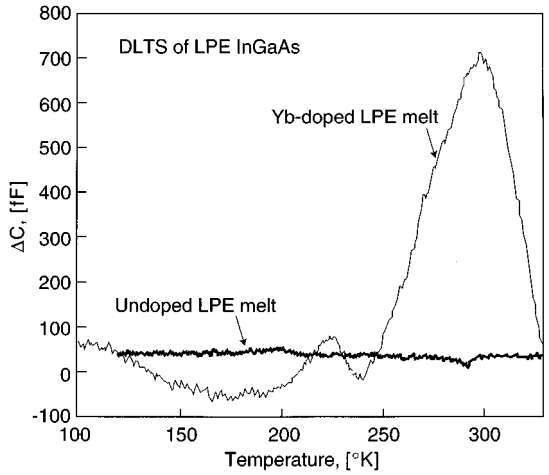

FIG. 9. Deep level transient spectra (DLTS) signal of electron traps in $In_{0.53}Ga_{0.47}As$ grown from an undoped (P11-1) and Yb-treated LPE melt (P11-3) on InP with 1 ms fill pulse. The addition of Yb doping to the LPE melt creates two deep levels at 225 and 295 K in the $In_{0.53}Ga_{0.47}As$ compared to the as-grown undoped $In_{0.53}Ga_{0.47}As$.

Takeda *et al.*,[21] even with Zn doping. Although Forrest and Kim[19] reported an electron trap with activation energy 0.17 eV and a density of $3-8 \times 10^{13}$ cm^{-3} in undoped LPE-grown $In_{0.53}Ga_{0.47}As$ on InP, Takeda stated that ''it can be speculated that InGaAs and InP grown by Forrest *et al.* had a poor crystal quality or that the measurement technique of the admittance spectroscopy could not separate the signal from the p–n junction and the heterointerface as indicated by Ogura *et al.* (1983).''[21] Figure 9 also displays the DLTS signal observed in $In_{0.53}Ga_{0.47}As$ epitaxial layer (P11-3) grown with the Yb-doped LPE melt. Here, two electron traps were observed. One was observed at 295 K, the other one at 225 K, which correspond to about 0.5–0.6 eV, 1.8×10^{11} cm^{-3} and 0.3–0.4 eV, 2×10^{10} cm^{-3} energy levels and peak densities, respectively. This is in good agreement with the C–V measurements.

Pal and Bose[22] observed a deep level in their Dy gettering LPE-grown n-$In_{0.53}Ga_{0.47}As$ layer, which had a capture cross section of 7×10^{-17} cm^{-2} and an activation energy of 0.32 eV. Pal and Bose believed the deep level is related to the incorporation of oxygen. As presented above, the oxygen level was enhanced after the rare-earth element treatment according to SIMS. Thus, oxygen is expected to be the deep level species at 0.3–0.4 eV. The other deep level at 0.5–0.6 eV is perhaps related to one of the detected impurities within the rare-earth element foils.

H. Glow discharge mass spectrometry

The purity of rare-earth elements is not typically equivalent to the high-purity In and Ga available for making LPE growth melts. Davis *et al.*[23] performed SIMS analysis of their Yb source and detected many impurities using SIMS, including Fe, Cr, Si, and Mg, etc. Unfortunately, they did not supply the concentrations of individual impurities.

Glow discharge mass spectrometry (GDMS) was used to measure the impurity levels in the rare-earth element foils used in this study. The measured impurity levels are then compared to the impurity levels measured by the vendor and supplied in their Certificate of Analysis. It is known that the Er and Yb vendor performs their analysis using optical emission spectrography during total combustion with a constant current dc arc. GDMS offers an alternative for measuring impurity levels. Table IV lists the impurities found at potentially 1 ppm or greater concentrations by GDMS in the Yb, Er, and Gd sources used in this study. Some selectivity of the impurity species being monitored was made prior to GDMS analysis. Emphasis was placed on known impurities given by the supplied Certificate of Analysis from the various vendors, as well as impurities which are known to create electrically active impurity levels. Therefore, the GDMS analysis did not scan every element within the periodic table, but the scans were very comprehensive. The GDMS system, a Fissons (VG-9000) magnetic sector instrument, used a flat-cell configuration using a discharge of 400 μA at 1000 V. No sample cleaning was performed prior to measurement except for a methanol wipe. Accuracy of the GDMS analysis is expected to be within 30%; however, sources of carbon, nitrogen and oxygen (residual atmospheric gases), and tanta-

TABLE IV. Impurities detected using glow discharge mass spectrometry in Er, Gd, and Yb foils and compared to the vendor supplied certificate of analysis.

Erbium			Gadolinium			Ytterbium		
Element	Conc. ppm	Certificate ppm	Element	Conc. ppm	Certificate ppm	Element	Conc. ppm	Certificate ppm
Ta	5400	7000	Yb	6300		O	620	
O	4900		O	4600		Ca	450	300
W	<1200		Ta	440		C	230	
C	630		La	200	150	Lu	86	<100
S	260		S	140		Zn	81	
Fe	260	200	C	120		Eu	72	
Nd	220		Y	110	70	Se	<67	
Re	<220		Si	56	2	S	28	
Tm	170	<100	Lu	42	30	Al	14	<100
Y	70	100	Cu	38	70	Mg	12	<100
Ti	67		Zr	34		Sm	12	
Cu	66		Tb	27		Nd	10	
Ni	65	<100	Ag	22		Si	10	200
Au	<63		Ce	17	100	Pr	9.1	
Ce	57		Fe	7.4	30	Os	< 7.4	
Si	47	<100	W	6.8		Ce	7.1	
Ge	34		Al	6	7	Gd	5.9	
Al	34	<100	Au	<5.7		Mn	4.4	
Lu	29		Pd	4.1		Y	3.4	<100
Ca	23	<100	Dy	4		Dy	3.4	
La	21		Er	3.2		La	3.4	
Gd	14		Nd	2.7		Ge	2.4	
Dy	11	<100	Ni	2.2		Ta	< 2.2	
Ho	11	<100	Zn	2		Tb	1.8	
Mn	10		Ir	<2		Te	< 1.7	
Pr	5.5		Se	<1.8		Ir	< 1.4	
Tb	4.5		Pt	1.5		Er	1.3	<100
Nb	3.1		Sm	1.4		Hg	< 1.1	
Sm	3.1		Tm	1.3				
Cr	2.7		Ge	<1.3				
Yb	1.3	<100						
Mo	<1.3							
Se	<1.3							
V	1.2							

lum (discharge cell) contamination are possible during the GDMS measurements.

The GDMS results shown in Table IV rank the impurity species by their relative detected abundance. From an inspection of these tables, it is noticeable that elements such as C and Zn which are known p-type dopants and other transition metals such as W, Ta, and Fe which are known to create deep level centers are some of the most abundant impurities. It is clear from earlier data that rare-earth treatment to an LPE melt acts to getter impurities and prevents them from accumulating into the grown epilayer; however, GDMS analysis shows that the rare-earth elements used in this study may also be a significant source of impurities. Since there is indication that the most dominant of these impurities are p-type dopants or sources of deep-level centers it helps to explain the measured Hall mobilities and carrier concentrations. There was an indication that the InGaAs samples which had undergone rare-earth treatment to the LPE melts were highly compensated due to the low 77 K mobility. This could be the case if the rare-earth elements were able to getter many species which act as n-type dopants with greater efficiency than those which act as p-type dopants or deep levels. Since Hall measurements only measure N_D-N_A, it is likely that the donor level has been shifted downward by the rare-earth gettering while the acceptor level has been somewhat enhanced by introduction of new impurities from the rare-earth foils. This could readily explain the extremely low net carrier concentrations ($\sim 10^{13}$ cm^{-3}) which were measured, while the mobilities were below state of the art.

IV. CONCLUSION

In conclusion, $In_{0.53}Ga_{0.47}As$ epilayers have been grown on semi-insulating (100) InP:Fe substrates. The growths were performed by LPE in a graphite boat using LPE melts doped with rare-earth species. The rare-earth elements studied were Yb, Gd, and Er. Due to the rare-earth elements' high reactivity, they act as gettering agents of impurities within the LPE melt by readily bonding to impurities (i.e., C, S, Si, Cu, and Fe). The reacted rare-earth species are insoluble in the LPE melts where In is used as the solvent. It is believed that precipitates of the reacted rare-earth elements form an insoluble slag on the surface of the LPE melt. In this manner, the LPE melt is cleansed and subsequent

$In_{0.53}Ga_{0.47}As$ epitaxial layer quality using LPE melts doped with trace amounts of rare-earth elements is dramatically improved. Hall measurements and PL studies confirm this point.

There is no indication from FTIR and x-ray-diffraction analysis that the rare-earth elements are incorporated into the crystal lattice which would manifest itself as a shift in band gap or lattice parameter. In fact, EDS and SIMS compositional studies were unable to find, within their detection limits, any rare-earth elements within the bulk $In_{0.53}Ga_{0.47}As$ epitaxial layers. EDS studies did indicate inclusion of rare-earth species inside particulate defect sites on the $In_{0.53}Ga_{0.47}As$ surface. Systematic compositional SIMS analysis of undoped and rare earth-treated $In_{0.53}Ga_{0.47}As$ samples reveal a reduction in many impurities which are attributed to doping centers and deep levels sites.

The low field mobilities measured at liquid-nitrogen temperatures and the almost unrealistic 9.33×10^{13} cm^{-3} background carrier concentration for rare-earth-treated $In_{0.53}Ga_{0.47}As$ samples suggest that these samples are compensated. Since Hall studies probe only N_D-N_A, it is speculated that the rare-earth treatments to the LPE melts preferentially getter n-type species. Also, it is believed that the background acceptor level rose slightly upon rare-earth treatment to the LPE melts. Final GDMS studies of the impurity levels in the commercially available rare-earth foils used in this study found high concentrations of impurities, many act as sources of p-type dopants and deep levels. DLTS measurements revealed the creation of two deep levels possibly from the rare-earth element itself, but more likely from impurities contained within the rare-earth foils. In conclusion, rare-earth treatment to the $In_{0.53}Ga_{0.47}As$ LPE melts improved layer quality, but impurities from the rare-earth element foils clouded the overall benefits of these rare-earth treatments.

ACKNOWLEDGMENTS

The authors would like to thank Joshua Burrill for some Hall measurements, Tom Goodwin for helpful discussions about the rare-earth treatments, and one author (W.G.) would like to thank Professor Robert G. Hunsperger for support and guidance as his thesis co-advisor.

[1] M. G. Astles, *Liquid-Phase Epitaxial Growth of III-V Compound Semiconductor Materials and Their Device Applications* (Adam Hilger, Bristol, England, 1990), pp. 25–36.
[2] Y. C. Lu, E. Bauser, and H. J. Queisser, J. Cryst. Growth **121,** 566 (1992).
[3] J. K. Rhee and P. K. Bhattacharya, J. Electrochem. Soc. **130,** 700 (1983).
[4] J. D. Oliver and L. F. Eastman, J. Electron. Mater. **9,** 693 (1980).
[5] E. Kuphal and A. Pocker, J. Cryst. Growth **58,** 133 (1982).
[6] P. K. Bhattacharya, M. V. Rao, and M-J. Tsai, J. Appl. Phys. **54,** 5096 (1983).
[7] N. T. Bagraev, L. S. Vlasenko, K. A. Gatsoev, A. T. Gorelenok, A. V. Kamanin, V. V. Mamutin, B. V. Pushnyul̆, V. K. Tibilov, Y. P. Tolparov, and A. E. Shubin, Sov. Phys. Semicond. **18,** 49 (1984).
[8] J. Haigh, in Proceedings of the 1980 NATO InP Workshop (1980), p. 123.
[9] G. S. Pomrenke, P. B. Klein, and D. W. Langer, Rare-earth Doped Semiconductors, Materials Research Society Symposium Proceedings, Vol. 301 (MRS, Pittsburgh, 1993).
[10] S. Adachi, J. Appl. Phys. **53,** 8775 (1982).
[11] C. P. Kuo, S. K. Vong, R. M. Cohen, and G. B. Stringfellow, J. Appl. Phys. **57,** 5428 (1985).
[12] I. C. Bassignana, C. J. Miner, and N. Puetz, J. Appl. Phys. **65,** 4299 (1989).
[13] W. H. Haydl, H. D. Muller, and H. Ennen, Appl. Phys. Lett. **46,** 870 (1985).
[14] A. T. Gorelenok, V. G. Gruzdov, R. Kumar, V. V. Mamutin, T. A. Polyanskaya, I. G. Savel'ev, and Y. V. Shmartsev, Sov. Phys. Semicond. **22,** 21 (1988).
[15] W. Körber, J. Weber, A. Hangleiter, K. W. Benz, H. Ennen, and H. D. Müller, J. Cryst. Growth **79,** 741 (1986).
[16] W. Gao, Ph.D. thesis, University of Delaware, 1995.
[17] P. S. Whitney, W. Lee, and C. G. Fonstad, J. Vac. Sci. Technol. B **5,** 796 (1987).
[18] S. Loualiche, A. Gauneau, A. Le Corre, D. Lecrosnier, and H. L'Haridon, Appl. Phys. Lett. **51,** 1361 (1987).
[19] S. R. Forrest and O. K. Kim, J. Appl. Phys. **53,** 5738 (1982).
[20] M. Ogura, M. Mizuta, K. Onaka, and H. Kukimoto, Jpn. J. Phys. **22,** 1502 (1983).
[21] Y. Takeda, S. Takigwa, M. Kasu, and A. Sasaki, in *International Symposium on GaAs and Related Compounds*, Karuizawa, Japan 1985, 301.
[22] D. Pal and D. N. Bose, J. Appl. Phys. **77,** 210 (1995).
[23] A. Davis, H. M. Dauplaise, J. P. Lorenzo, G. O. Ramseyer, and J. A. Horrigan, in *Materials Research Society Symposium Proceedings*, San Francisco, CA (MRS, Pittsburgh, 1993), Vol. 301, pp. 151–162.